Calculation of Reactive Cross Sections and Microcanonical Rates from Kinetic and Thermochemical Data

Jan P. Hessler*

Chemistry Division, Argonne National Laboratory, 9700 South Cass Avenue, Argonne, Illinois 60439-4831

Received: April 25, 1997; In Final Form: March 25, 1998

In general, kinetic rate data may be represented by van't Hoff's four-parameter equation. When this is true, the mathematical properties of the Laplace transform may be used to derive phenomenological equations that describe the energy-dependent reactive cross sections and microcanonical rates in terms of the same four parameters. Since the macroscopic rate data and microscopic expressions are related by the Laplace transform, these microscopic descriptions do not imply new information; they simply express the information contained in the rate data in another form. The Monte Carlo techniques used to determine confidence envelopes for the rate data may also be used to provide confidence envelopes or "bounds" for the energy-dependent properties. These microscopic expressions may be used to compare and contrast theoretical calculations or as a starting point in RRKM or master equation calculations. Both the forward and reverse $H + O_2 \leftrightarrow OH + O$ reactions and the associative reaction $CH_3 + CH_3 \rightarrow C_2H_6$ are used to illustrate the above ideas. In the first example, the cross section for the reverse reaction shows that it is not dominated by the dipole−quadrupole interaction. The cross section for the forward reaction is obtained by fitting rate data from 158 to 5300 K and peaks just above the threshold of 8354 K. In the second example, comparison to recent theoretical calculations highlights the importance of angular momentum and the centrifugal barrier.

I. Introduction

Thermal rate constants are one of the most important properties for chemical reactions. They are needed to model the chemistry of the atmosphere, combustion, and waste incineration. In general, experimental measurements of the temperature dependence of the rate constant are reduced by least-squares analysis.[1] The best-fit parameters from this reduction along with their associated uncertainties and correlations are then used to produce reaction mechanisms that are used to model complex chemical systems. Three calculations are generally needed to compare measurements to theoretical predictions. First, the potential energy surface must be calculated.[2] Second, transition state theory,[3] or one of its modern variants,[4−6] is used to approximate the energy and angular momentum resolved rate, $k(E, J)$. To overcome the approximate nature of these calculations Yamamoto[7] and Miller[5,8] introduced the reactive flux correlation function to calculate exactly the cumulative reaction probability, $N(E)$. Finally, these energy-dependent descriptions are related to the rate constant *via* Boltzmann's average and the reactant partition function. The goal of this work is to use experimental temperature-dependent kinetic and thermochemical data to provide phenomenological descriptions of the energy dependence of chemical reactions. These descriptions can then be compared to measurements of the reactive cross section and theoretical calculations of $k(E, J)$ or $N(E)$. They may also be used to classify reactions or as starting points for the calculation of pressure-dependent rates in the falloff region of associative and dissociative reactions.

In this work, the mathematical properties of the Laplace transform are used to derive phenomenological expressions for reactive cross sections and microcanonical rates in terms of the parameters used to describe the rate data. These expressions may be viewed as alternate descriptions of the data.[9] As such, they do not contain information that is not in the data; the information is simply presented in a different form. Previously, Menzinger and Wolfgang[10] discussed a number of forms of energy-dependent reactive cross sections and LeRoy[11] discussed the implications of three general forms of the reactive cross section. Here, an alternate approach is presented. We assume the kinetic data are adequately described by van't Hoff's (1898) equation,[12] $k(T) = AT^m \exp[-(E + DT^2)/T]$. The inverse Laplace transform is used to derive an analytic expression for the thermally averaged cross section in terms of the parameters of van't Hoff's equation: A, m, E, and D. The need stressed by Polanyi and Schreiber,[13] for "bounds" on the cross section, can be answered with this expression and the Monte Carlo techniques[14] that are used to assign confidence envelopes to the kinetic data. The philosophy behind this work is that kinetic experiments are limited to one or at most two dimensions, temperature and pressure, and that all experimental data have uncertainties. Therefore, within the limitations of bulk experiments and their associated uncertainties, we wish to extract the maximum amount of information about a reaction. This information can be displayed both as a temperature-dependent rate coefficient and as an energy-dependent cross section or microcanonical rate. For both of these descriptions the experimental uncertainties may be used to generate realistic limits for the information. In the next section, the phenomenological equations for the reactive cross section and microcanonical rate are derived. In addition, for reactions that have a negative temperature dependence that may be described by Berthelot's (1862) equation,[15] $A \exp(-DT)$, the parameter D is shown to characterize an effective barrier that depends upon the internal temperature of the reacting species. In section III, data for the forward and reverse rates of the reaction $H + O_2 \leftrightarrow OH + O$

* Address correspondence to this author. Voice: 1-630-252-3717. Facsimile: 1-630-252-4470. E-mail: hessler@anl.gov.

S1089-5639(97)01416-3 CCC: $15.00
Published on Web 05/15/1998

are analyzed to determine the thermally averaged cross sections and their confidence envelopes. The formulation used to reduce the kinetic data[16] and the Monte Carlo simulations[14] needed to calculate confidence envelopes are briefly described. Data that span different temperature ranges are used to demonstrate how extending the temperature range of kinetic measurements improves the confidence envelopes for both the rate data and the cross section. Finally, data for the high-pressure rate of the associative reaction $CH_3 + CH_3 \rightarrow C_2H_6$ are analyzed and microcanonical rates are calculated. These compare favorably to a direct variational RRKM calculation of the energy and angular momentum resolved rates,[17] which is based on 8000 points from a recent *ab initio* calculation of the potential energy surface.[18] In section IV, general implications of the derivations and examples are discussed.

II. Derivation

A. Bimolecular Reactions. The concept of a cross section has been used to describe collisions between atoms and molecules,[19] absorption of particles by nuclei,[20] and chemical reactions.[21] The general equation for a rate coefficient, k, in terms of an energy-dependent cross section, $\sigma(\epsilon_t)$, for structureless particles is given by

$$k(T_t) = \left(\frac{8}{\pi\mu(k_B T_t)^3}\right)^{1/2} \int_0^\infty \epsilon_t \sigma(\epsilon_t) \exp(-\epsilon_t/k_B T_t)\, d\epsilon_t \quad (1)$$

where the reduced mass of the species is μ, Boltzmann's constant is k_B, the translational energy is ϵ_t, and the subscript "t" has been added to the temperature to denote that it characterizes the distribution of the translational energies of the colliding species. If the particles have structure, *i.e.*, electronic, rotational, and vibrational levels, the above equation can be rewritten as

$$k(T_t, \gamma_1, \gamma_2) = \left(\frac{8}{\pi\mu(k_B T_t)^3}\right)^{1/2} \int_0^\infty \epsilon_t \sigma(\epsilon_t, \gamma_1, \gamma_2) \times \exp(-\epsilon_t/k_B T_t)\, d\epsilon_t \quad (2)$$

where γ_1 and γ_2 are the sets of electronic, rotational, and vibrational quantum numbers for each of the reactive species. In a kinetic experiment, the quantum levels of the reactive species cannot be selected. Therefore, their populations are assumed to be given by Boltzmann's distribution, which is characterized by an internal temperature, T_{int}. Under some conditions it may be necessary to characterize the populations by different temperatures, *e.g.*, an electronic, a vibrational, and a rotational temperature. However, to simplify this discussion all of these are set equal to T_{int}. Therefore, the thermally averaged rate coefficient may be written

$$k(T_t, T_{int}) = \frac{1}{Q_{12}} \sum_{i,j=1}^{\infty} g_{1i} g_{2j} k(T_t, \gamma_{1i}, \gamma_{2j}) \exp[-(E_{1i} + E_{2j})/k_B T_{int}] \quad (3)$$

while the thermally averaged cross section is written

$$\sigma(\epsilon_t, T_{int}) = \frac{1}{Q_{12}} \sum_{i,j=1}^{\infty} g_{1i} g_{2j} \sigma(\epsilon_t, \gamma_{1i}, \gamma_{2j}) \exp[-(E_{1i} + E_{2j})/k_B T_{int}] \quad (4)$$

The partition function, Q_{12}, is given by

$$Q_{12} = \sum_{i,j=1}^{\infty} g_{1i} g_{2j} \exp[-(E_{1i} + E_{2j})/k_B T_{int}] \quad (5)$$

where the coefficients g_{1i} and g_{2j} represent the degeneracies and E_{1i} and E_{2j} the energies of the levels of species 1 and 2, respectively. With these definitions,[22] eq 2 may be written

$$k(T_t, T_{int}) = \left[\frac{8}{\pi\mu(k_B T_t)^3}\right]^{1/2} \int_0^\infty \epsilon_t \sigma(\epsilon_t, T_{int}) \exp(-\epsilon_t/k_B T_t)\, d\epsilon_t \quad (6)$$

In general, T_{int} and T_t will be equal, but to differentiate between the distributions of the translational and internal energies the subscripts are retained.

The most useful analytic description of temperature-dependent rate data is given by van't Hoff's (1898) equation.[15] Although van't Hoff did not distinguish between internal and translational temperatures, his equation may be written to retain this distinction. His modified equation is

$$k(T_t, T_{int}) = A(k_B T_t)^m \exp[-(E + Dk_B^2 T_{int}^2)/k_B T_t] \quad (7)$$

This modification is justified by the fact that the parameter E is associated with the threshold of the reaction. This and all other properties that distinguish one reaction from another must be contained in the potential energy surface and, therefore, cannot depend upon the translational energy of the species. It follows that the parameter D, which is associated with Berthelot's (1862) equation,[15] must depend upon the potential energy surface and not the translational energy. This approach is analogous to the use of an "effective" potential to account for the centrifugal barrier at different values of the impact parameter.[23] Also, note that Boltzmann's constant has been introduced into the pre-exponential temperature term; the dimension of the coefficient A is $length^3 time^{-1} energy^{-m}$. For convenience, and to more clearly separate internal and translational aspects, the notation may be changed and eq 7 may be rewritten as

$$k(T_t, E_{eff}) = A(k_B T_t)^m \exp[-E_{eff}/k_B T_t] \quad (8)$$

where

$$E_{eff} = E + Dk_B^2 T_{int}^2 \quad (9)$$

This is equivalent to Kooij's (1893) equation,[15] but with an effective energy that depends upon the distribution of internal energy of the reacting species. Of course, a more complex equation for the effective energy could be invoked. However, one must first establish that the additional complexity is needed to reproduce the data. When eqs 6 and 8 are combined one obtains

$$A(k_B T_t)^{m+3/2} \exp(-E_{eff}/k_B T_t) = \left(\frac{8}{\pi\mu}\right)^{1/2} \int_0^\infty \epsilon_t \sigma(\epsilon_t, E_{eff}) \times \exp(-\epsilon_t/k_B T_t)\, d\epsilon_t \quad (10)$$

From a table of Laplace transforms,[24] the thermally averaged reactive cross section is given by

$$\sigma(\epsilon_t, E_{eff}) = A\left(\frac{\pi\mu}{8}\right)^{1/2} \frac{(\epsilon_t - E_{eff})^{m+1/2}}{\epsilon_t \Gamma(m + {}^3/_2)} \Theta(\epsilon_t - E_{eff}) \quad (11)$$

where $m > -{}^3/_2$, the unit step function is $\Theta(\epsilon_t - E_{eff})$, and the

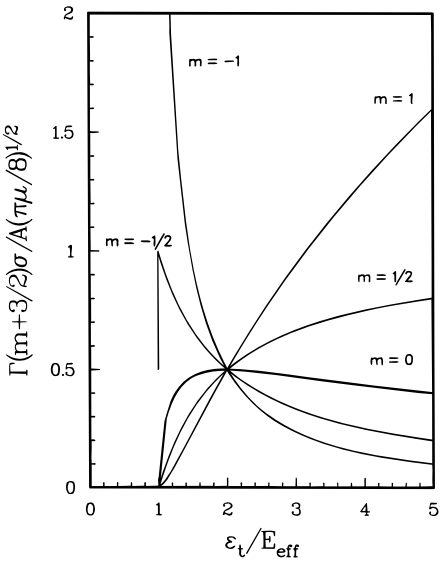

Figure 1. Normalized cross section as a function of ϵ_t/E_{eff} for various values of the parameter m. See the text for details.

Γ function is $\Gamma(m + {}^3/_2)$. Since A has the dimension $length^3 time^{-1} energy^{-m}$, then $\sigma(\epsilon_t, E_{eff})$ has the dimension $length^2$, as it should.

Equation 11 implies that if kinetic rate data can be described by equation 7 or 8 then the reactive cross section can be described by the same parameters. Since this cross section is related to the kinetic data through the Laplace transform, additional information has not been produced; the information contained in the kinetic data has simply been transformed. This transformation is analogous to the fact that quantum mechanical systems may be described either in coordinate or momentum space. The two representations of quantum systems are related by the Fourier transform, while for thermal kinetic systems the temperature-dependent rate coefficient and the energy-dependent cross section are related by the Laplace transform. In 1974,[13] Polanyi and Schreiber stated "What is needed is some method of obtaining the bounds on the cross section". Later, when the $H + O_2 \leftrightarrow OH + O$ reactions are considered, we shall demonstrate how thermochemical and kinetic data may be combined to obtain a self-consistent set of data and how Monte Carlo simulations that are used to determine confidence envelopes for the rate data can also be used to generate confidence envelopes, or "bounds", for the cross section. These bounds reflect the fact that the experimental data are available only over a finite temperature range.

Before proceeding, it is instructive to look at the behavior of eq 11. If $m \leq -{}^3/_2$, the Laplace transform is not valid. For $-{}^3/_2 < m < -{}^1/_2$ the cross section has an integrable singularity at $\epsilon_t = E_{eff}$ and decays rapidly as ϵ_t increases. This is demonstrated by the curve labeled $m = -1$ in Figure 1. For $m \geq -{}^1/_2$ the cross section is no longer singular. At $m = -{}^1/_2$ the dependence upon energy falls off as $1/\epsilon_t$ and is shown by the curve labeled $m = -{}^1/_2$. For $-{}^1/_2 < m < {}^1/_2$ the cross section increases from zero at $\epsilon_t = E_{eff}$, peaks at $\epsilon_t = 2E_{eff}/(1 - 2m)$, and then decays to zero as $\epsilon_t \rightarrow \infty$. At $m = 0$ van't Hoff's expression of 1884, which was later reproduced by Arrhenius in 1889,[12] $A \exp(-E_{eff}/k_B T_t)$, is obtained. Here, the cross section peaks at $\epsilon_t = 2E_{eff}$. For $m = {}^1/_2$ the simple collision expression of Lewis and Trautz, which reaches a maximum as $\epsilon_t \rightarrow \infty$, is recovered. For $m > {}^1/_2$ the cross section rises monotonically from $\epsilon_t = E_{eff}$; this is shown as the curve labeled $m = 1$. It is important to note that the parameter m, and only m, controls the shape of the cross section, while A determines its magnitude and E_{eff} determines the location of the singularity or its origin. At this point, we consider the Wigner threshold law for reactions that proceed over a threshold.[25] This law states that in the threshold region

$$\sigma(\epsilon_t, l) \propto (\epsilon_t - E_{eff})^{(2l+1)/2} \tag{12}$$

where the relative angular momentum of the reacting species is $l = 0, 1, 2,$ *etc.* Just above threshold the additional centrifugal barrier limits the contribution from high angular momentum states so that $l = 0$, the *s*-wave state, dominates. Therefore, the integrable singularity that occurs for $m \leq -{}^1/_2$ violates Wigner's threshold law. From this we conclude that data that produce a best-fit m that is less than $-{}^1/_2$ must be interpreted cautiously. Above the threshold region the chemical potential controls the reactivity and, therefore, the value of m. Since all of the curves in Figure 1 intersect at $\epsilon_t/E_{eff} = 2$, the parameter m can be determined from collisions with $E_{eff} \leq \epsilon_t \leq 2E_{eff}$. Therefore, when E_{eff} has a finite value the shape of the cross section can be determined from kinetic data up to $T_t \sim 4E_{eff}/k_B$. When $E_{eff} \rightarrow 0$ most of the collisions will have kinetic energies greater than $2E_{eff}$ and it will be important to obtain data at as low a temperature as possible. Of course, in either case, the larger the temperature range of the data the more precisely m will be determined. This observation may appear to be in conflict with conventional wisdom that states measurements must be performed over an infinite temperature range to obtain information about the behavior of the reactive cross section. This apparent conflict can be resolved when one realizes that conventional wisdom is based upon the fact that numerical calculations of inverse Laplace transforms are exceedingly difficult.[26] However, in this case, measurements over a finite temperature range are replaced by the assumption that if eq 7 or 8 adequately reproduces the data over a range of temperatures it will continue to be adequate at lower and higher temperatures. An alternate way of looking at this problem is that if kinetic data are available over a sufficiently large temperature range, *e.g.*, over the temperature range needed to model atmospheric, combustion, or incineration processes, and if the data are adequately fit by eq 7 or 8, then eq 11 is an adequate description of the energy-dependent cross section. The term adequate may be quantitatively defined in terms of confidence envelopes, which will be discussed later.

To derive a phenomenological expression for the microcanonical rate, $k(\epsilon_t, E_{eff})$, recall that it is related to the canonical or macroscopic rate, $k(T_t, E_{eff})$, through

$$k(T_t, E_{eff}) = \frac{1}{Q(T_t)} \int_0^\infty \rho(\epsilon_t)\, k\,(\epsilon_t, E_{eff}) \exp(-\epsilon_t/k_B T_t)\, d\epsilon_t \tag{13}$$

where the translational partition function per unit volume is $Q(T_t)$, which is given by

$$Q(T_t) = \frac{(2\pi\mu k_B T_t)^{3/2}}{h^3} \tag{14}$$

Since the partition function is the Laplace transform of the translational density of states per unit volume, $\rho(\epsilon_t)$, it follows that

$$\rho(\epsilon_t) = \frac{4\sqrt{2}\pi\mu^{3/2}}{h^3}\epsilon_t^{1/2} \tag{15}$$

Therefore, one can immediately write the thermally averaged microcanonical rate as

$$k(\epsilon_t, E_{eff}) = [2/\mu]^{1/2}\epsilon_t^{1/2}\sigma(\epsilon_t, E_{eff}) \quad (16)$$

where the thermal average is over the internal degrees of freedom of the reacting species. From eq 11 we have

$$k(\epsilon_t, E_{eff}) = \frac{A}{2}\pi^{1/2}\frac{(\epsilon_t - E_{eff})^{m+1/2}}{\epsilon_t^{1/2}\Gamma(m + {}^3/_2)}\Theta(\epsilon_t - E_{eff}) \quad (17)$$

Again, eq 17 implies that if kinetic rate data can be described in terms of eq 7 or 8 then a thermally averaged microcanonical rate can be described by the same parameters. In addition, confidence envelopes or "bounds" may also be calculated for this rate.

B. Associative Reactions. The high-pressure limit of associative reactions may be written as a simple bimolecular reaction.[27,28] Therefore, the microcanonical rate for association is given by eq 17. Some associative reactions proceed on a barrierless potential energy surface, *e.g.*, $H + CH_3$ and $CH_3 + CH_3$. Previously[14] it had been demonstrated that the high-pressure limit of methyl−methyl association has a negative temperature dependence that is best described by Berthelot's (1862) equation.[15] Neither the Harcount−Essen equation of 1895, AT^{-m}, nor Kooij's (1893) equation, $AT^{-m}\exp(-E/k_BT)$, provides an adequate description of these data. Therefore, it is important to assign physical significance to the parameter D in Berthelot's equation, which from eq 7 we write as $A\exp(-Dk_BT_{int}^2/k_BT_t)$ since both E and m are zero. First, consider the expression for the associative microcanonical rate, eq 17, in the limit of zero internal energy, $T_{int} \rightarrow 0$. Then

$$k\infty_{asso}(\epsilon_t, E_{eff} \rightarrow 0) = A \quad (18)$$

For a finite value of the internal temperature the microcanonical rate becomes

$$k\infty_{asso}(\epsilon_t, E_{eff} \rightarrow Dk_B^2T_{int}^2) = A\left(1 - \frac{Dk_B^2T_{int}^2}{\epsilon_t}\right)^{1/2}\Theta(\epsilon_t - Dk_B^2T_{int}^2) \quad (19)$$

At high translational energies, $\epsilon_t \gg Dk_B^2T_{int}^2$, this rate approaches A. At translational energies comparable to the internal energies of the species, $\epsilon_t \sim Dk_B^2T_{int}^2$, an effective threshold to association exists and depends upon the internal energy contained within the associating species. Therefore, the parameter D characterizes a temperature-dependent effective barrier

$$E_{eff} = Dk_B^2T_{int}^2 \quad (20)$$

that is due to the internal energy of the species. This barrier is analogous to the centrifugal barrier.[23] As was stated above, the parameter m, and only m, controls the shape of the cross section. Therefore, it also controls the shape of the microcanonical rate. For Berthelot's equation m is fixed at zero. Therefore, the only way Berthelot's equation can reproduce any temperature dependence is through a temperature-dependent E_{eff}.

It is well-known that it is difficult to extract the high-pressure limit of associative reactions from experimental data; as the temperature is increased, exceedingly high pressures are needed. In general, this limit is obtained by assuming an analytic expression for the pressure-dependent behavior in the falloff region[29] and reducing the data with a nonlinear least-squares fit.[30] An advantage of the approach presented here is that the microcanonical rate given by eq 17 may be used as a starting point for calculating rates in the falloff region. Either standard RRKM techniques or a one-dimensional master equation[31] may be used to calculate pressure-dependent rates. These calculated rates may then be compared to measured rates and a best-fit set of parameters may be determined. With this approach, it will be possible to extract simultaneously the parameters of eq 7 for the high-pressure rate coefficient and the parameters needed to describe the pressure-dependent behavior. In addition, the experimental uncertainties may be used with Monte Carlo simulations to calculate confidence envelopes for the high-pressure rate coefficient, the microcanonical rate, and the macroscopic rates.

III. Illustrations

A. Bimolecular Reactions. To illustrate the above concepts consider the elementary reactions between hydrogen, oxygen, and the hydroxyl radical. The reaction $H + O_2 \rightarrow OH + O$ is the most important reaction in combustion and has been measured from 962 to 5300 K. The reverse reaction, $OH + O \rightarrow H + O_2$, is important in modeling stratospheric and interstellar chemistry and has been measured from 158 to 515 K. The first measurements of the reverse reaction were reported by Lewis and Watson and covered the temperature range 221−499 K.[32] Shortly thereafter,[33] Howard and Smith reported measurements from 250 to 515 K and Brune, Schwab, and Anderson performed measurements at 300 K.[34] Recently, Smith and Stewart extended measurements down to 158 K.[35] Unfortunately, the data of Lewis and Watson and the two sets from Smith's group do not overlap. The two sets from Smith's group will be used for this illustration.

The different spin−orbit states of the reactants of the reverse reaction produce a temperature-dependent contribution that complicates analysis of the measured rate coefficients. Spin−orbit effects may be introduced into the rate coefficient[36] by defining a hypothetical rate coefficient and writing

$$k_{hypo}(T) = F_{el}(T)k_{meas}(T) \quad (21)$$

where $F_{el}(T)$ accounts for the electronic degeneracy of the reactants, $k_{meas}(T)$ is the measured rate coefficient, and $k_{hypo}(T)$ represents the rate coefficient of the hypothetical reaction that proceeds on a single potential energy surface. The correction factor $F_{el}(T)$ is given by

$$F_{el}(T) = \left\{\frac{1}{Q_O(T)}\right\}\left\{\frac{1}{1 + \dfrac{Q_{rot}(^2\Pi_{1/2})}{Q_{rot}(^2\Pi_{3/2})}}\right\} \quad (22)$$

where the partition function of the oxygen atom is $Q_O(T)$ and the rotational partition functions for the different spin−orbit states of hydroxyl are $Q_{rot}(^2\Pi_{1/2})$ and $Q_{rot}(^2\Pi_{3/2})$. The rate coefficients for the hypothetical reaction are given in Table 1 and Figure 2. The negative temperature dependence of the hypothetical rate coefficient and the fact that the reaction proceeds on a barrierless potential energy surface[37] suggest that a different empirical expression, which accommodates behavior in the quantum threshold region, should be used to reduce the data.[38] However, in this system the quantum threshold region extends only up to 1 K. Therefore, the data are in the high-temperature region where the Harcourt−Essen equation,[15] AT^m, is appropriate. Berthelot's equation,[15] $A\exp(-DT)$, is also appropriate. The data were reduced by nonlinear least-squares techniques with a dimensionless formulation.[16] The best-fit

TABLE 1: Measured, Hypothetical, and Forward Rate Coefficients for O + OH

T, K	k_{meas},[a] cm^3 s^{-1}	F_{el}	k_{hypo}, cm^3 s^{-1}	k_{fwd}, cm^3 s^{-1}
158	$(6.10 \pm 0.60) \times 10^{-11}$	7.41	$(45.2 \pm 4.4) \times 10^{-11}$	8.14×10^{-33}
190	$(5.20 \pm 0.30) \times 10^{-11}$	8.13	$(42.3 \pm 2.4) \times 10^{-11}$	5.38×10^{-29}
227	$(4.50 \pm 0.30) \times 10^{-11}$	8.88	$(40.0 \pm 2.7) \times 10^{-11}$	6.37×10^{-26}
250	$(4.04 \pm 0.18) \times 10^{-11}$	9.30	$(37.6 \pm 1.7) \times 10^{-11}$	1.74×10^{-24}
294	$(4.20 \pm 0.20) \times 10^{-11}$	10.02	$(42.1 \pm 2.0) \times 10^{-11}$	2.82×10^{-22}
300	$(3.53 \pm 0.31) \times 10^{-11}$	10.11	$(35.7 \pm 3.1) \times 10^{-11}$	4.22×10^{-22}
375	$(3.36 \pm 0.24) \times 10^{-11}$	11.10	$(37.3 \pm 2.7) \times 10^{-11}$	1.12×10^{-19}
445	$(3.10 \pm 0.27) \times 10^{-11}$	11.84	$(36.7 \pm 3.2) \times 10^{-11}$	3.59×10^{-18}
515	$(2.76 \pm 0.14) \times 10^{-11}$	12.44	$(34.3 \pm 1.7) \times 10^{-11}$	4.23×10^{-17}

[a] References 33 and 35.

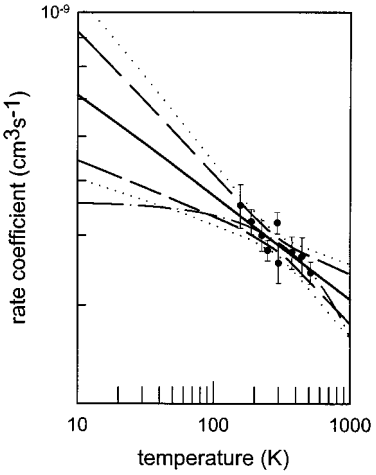

Figure 2. Measured rate coefficients for the reaction OH + O → H + O_2. The best-fit curve, eq 23, is given by the solid line. The 68.3% confidence envelope is shown by the dashed lines and the 95.4% envelope by the dotted lines. The data represented by the filled circles are from refs 33 and 35.

TABLE 2: Statistical Results for the Least-Squares Analysis of O + OH → H + O_2

eq	χ^2	χ^2_{red}	std dev	skewness	kurtosis
23	5.94	0.85	0.86	+0.39	−0.47
24	6.17	0.88	0.88	−0.01	−0.95

results with the Harcourt−Essen equation are

$$k_{hypo}(\text{cm}^3\ \text{s}^{-1}) = 7.4 \pm 1.5 \times 10^{-10} T(\text{K})^{-0.192 \pm 0.055} \quad (23)$$

The correlation coefficient between the two parameters is 0.998; this indicates a near maximum correlation. The best-fit parameters for Berthelot's equation are

$$k_{hypo}(\text{cm}^3\ \text{s}^{-1}) = (4.59 \pm 0.26) \times 10^{-10} \exp\{[(-5.6 \pm 1.7) \times 10^{-4}] T(\text{K})\} \quad (24)$$

The correlation coefficient between the two parameters is 0.938, which, again, indicates a near maximum correlation. The uncertainties listed above are the standard deviations determined by Monte Carlo simulations.[14] The values of χ^2, $\chi^2_{red} \equiv \chi^2$/(number of degrees of freedom), and the moments of the normalized residuals are given in Table 2. The lower value of χ^2 for eq 23 suggests that it provides a better representation of the data. However, inspection of the values of χ^2_{red} shows they are both less than 1.0. Therefore, the data are not precise enough to select one equation over the other. This is shown graphically in Figure 2 where the solid line represents eq 23 and the dash−dot−dash line eq 24. It is immediately clear that data down to 20 K will significantly improve the experimental description of this reaction. For the remainder of this illustration we shall consider only the results of the Harcourt−Essen equation.

Since confidence envelopes can only be obtained from Monte Carlo simulations,[14] a brief description follows. They are performed by generating several sets of simulated data. To generate a set each measured point is randomly varied within a Gaussian (normal) distribution with its standard deviation. These simulated data are then reduced to produce a set of best-fit parameters. These parameters are then related to the original data by calculating the χ^2 merit function with the new best-fit parameters and the original data. This value of χ^2 will be greater than the value calculated with the original data. The difference between these is denoted $\Delta\chi^2$ and stored along with the new set of parameters. After a sufficiently large number of simulations have been performed, histograms and scatter plots of the fractional changes in the parameters may be displayed and the standard deviations, skewness, kurtosis, and correlation coefficients calculated. Confidence envelopes are generated by sorting the values of $\Delta\chi^2$ in ascending order, while the parameters associated with each are retained. Then, for a desired temperature range, the locus of points of $k_{min}(T)$ and $k_{max}(T)$ are calculated from the sets of parameters associated with the lower 68.3 or 95.4% of the values of $\Delta\chi^2$. The curves defined by the locus of the $k_{min}(T)$ and $k_{max}(T)$ values define the confidence envelope of the rate coefficient. Since the temperature range may exceed the range of the measurements, this approach may be used to obtain realistic uncertainties in regions where data have not been obtained. Furthermore, in general, it is not possible to describe either $k_{min}(T)$ or $k_{max}(T)$ by a simple analytic function. The 68.3 and 95.4% confidence envelopes for the reverse rate are shown as the dashed and dotted lines, respectively, in Figure 2. A close inspection shows that over the temperature range of the data the dash−dot−dash line falls within the 68.3% confidence envelope of the solid line. This lends further support to our conclusion that the data are not precise enough to select one representation of the data over the other.

Now that an analytic expression for the rate coefficient and its confidence envelope have been determined, the reactive cross section may be calculated. The analytic expression for the reactive cross section, eq 11, is used with the parameters of eq 23 to produce the cross section shown as the solid line in Figure 3. Just as the confidence envelope for the rate expression is determined from the sets of parameters from the Monte Carlo simulations, the confidence envelope for the cross section is given by the locus of points defined by σ_{min} (ϵ_t) and σ_{max} (ϵ_t). The 95.4% confidence envelope for the cross section is shown by the dotted lines in Figure 3. This thermally averaged cross section, which has been calculated only from experimental data, may be compared to an analytic fit to the quantum-mechanical cross section determined by Graff and Wagner,[37] the dash−dot−dot line in Figure 3, the cross section calculated in the adiabatic capture infinite-order sudden approximation by Clary and Werner,[36] the dashed line, and the state-to-state calculations of Marques, Wang, and Varandas,[39] the circles with vertical lines. At these relatively high energies the quantum-mechanical calculation of Graff and Wagner scales as $\epsilon_t^{-1/2}$, which is consistent with the long-range dipole−quadrupole interaction. The cross section calculated from the kinetic data scales as $\epsilon_t^{-0.692 \pm 0.055}$, which implies that the reaction is controlled by the chemical potential. Note, although the theoretical and experimental cross sections agree near $\epsilon_t/k_B \sim 100$ K, the theoretical cross sections calculated by Graff and Wagner and Clary and Werner are outside the 95.4% confidence interval

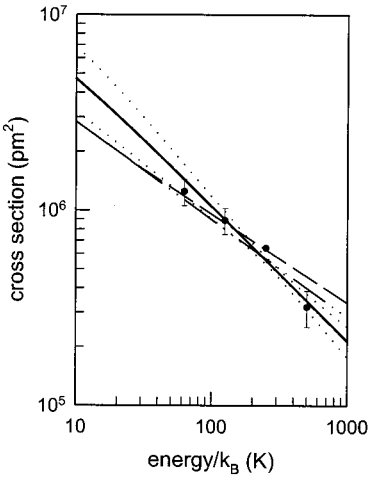

Figure 3. Cross section for the reverse reaction OH + O → H + O_2. The solid line is calculated with the parameters of eq 23 and the dotted lines represent the 95.4% confidence envelope. The dash−dot−dot line represents the calculation of Graff and Wagner[37] and the dashed line the calculation of Clary and Werner.[36] The vertical lines represent the range of *J* values of the state-to-state calculations by Marques, Wang, and Varandas.[39]

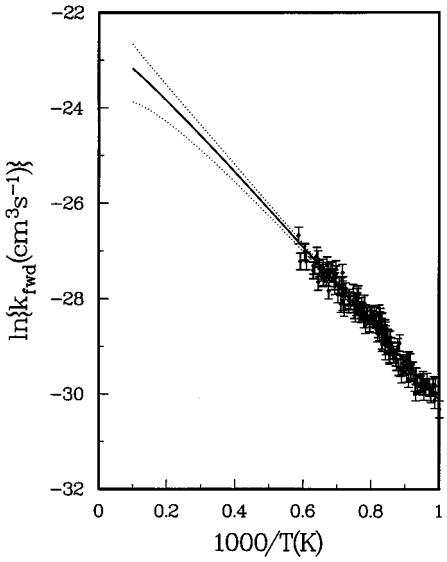

Figure 4. Lower temperature data for the rate of the reaction H + O_2 → OH + O. The solid line represents eq 25 and the dotted lines the 95.4% confidence envelope. The data are from ref 41 and Table 1. See the text for details.

for $\epsilon_t/k_B \leq 60$ K and $\epsilon_t/k_B \geq 300$ *K*. Conversely, the calculations by Marques, Wang, and Varandas fall within the experimental confidence envelope. This agreement between theoretical calculations and experimental measurements is even more remarkable when we recall that there is no adjustable parameter to scale either theoretical or experimental results.

To begin the discussion of the forward reaction, note that both the forward and reverse reactions are elementary. Therefore, the equilibrium constant may be used to relate their rate coefficients.[40] Table 1 also shows the calculated forward rate coefficients. Although the measured rate coefficients of the reverse reaction change by less than an order of magnitude, the forward rate coefficients change by over 15 orders of magnitude between 158 and 515 K. Therefore, almost all of the temperature dependence of the calculated forward rate coefficients may be associated with the temperature dependence of the equilibrium constant. Furthermore, since the partition functions of the reactants and products change very little at these low temperatures, the temperature dependence of the equilibrium constant is dominated by the change in molar enthalpy of the reaction, $\Delta H_0^0/R = 8317 \pm 156$ K.[40] To assure that the high-temperature data are consistent with both the thermochemical data and the lower temperature measurements of the reverse rate coefficients, the calculated forward rate coefficients will be combined with direct high-temperature measurements of the forward rate coefficients. The rate coefficient for the forward reaction was measured from 946 to 1705 K by Pirraglia, Michael, Sutherland, and Klem.[41] Master, Hanson, and Bowman measured the rate of formation of hydroxyl between 1450 and 3370 K and extracted the forward rate coefficient.[42] We also monitored hydroxyl to determine rate coefficients from 2050 to 5305 K.[43] Later, Ryu, Hwang, and Rabinowitz performed additional measurements between 1050 and 2500 K and discussed the work of other researchers.[44] For this illustration, only our high temperature data, the data of Masten, Hanson, and Bowman, and the data of Pirraglia, Michael, Sutherland, and Klem will be used. Each set of data was tested to determine if it was consistent with the calculated low-temperature rate coefficients and the thermochemical data. The three sets used in this illustration meet these criteria.

The high-temperature data will be analyzed in two steps to illustrate how an increase in the temperature range of the data improves the confidence envelopes for both the rate and its cross section. First, the data of Pirraglia, Michael, Sutherland, and Klem are combined with the calculated rate coefficients at lower temperatures, Table 1. The results of a nonlinear least-squares fit give

$$\ln\{k_{fwd}(\mathrm{cm^3\,s^{-1}})\} = -(19.36 \pm 0.88) - (0.35 \pm 0.12)\ln\{T(\mathrm{K})\} - (8345 \pm 61)/T(\mathrm{K}) \quad (25)$$

TABLE 3: Statistical Results for the Least-Squares Analysis of H + O_2 → OH + O

eq	χ^2	χ^2_{red}	std dev	skewness	kurtosis
25	157.9	0.97	0.98	−0.052	−0.46
26	211.0	0.96	0.97	+0.034	−0.51

The uncertainties above are the standard deviations calculated from the Monte Carlo simulations. The values of χ^2, $\chi^2_{red} \equiv \chi^2$/(number of degrees of freedom), and the moments of the normalized residuals are given in Table 3. The data, the best-fit curve, and the 95.4% confidence envelope are shown in Figure 4. To illustrate uncertainties in the high-temperature behavior of the rate coefficient, the best-fit curve and confidence envelope have been extended up to 10 000 K. At the 95.4% confidence level the parameter *m* extends from −0.63 to +0.06. Therefore the shape of the cross section will fall between the $m = -1/2$ and $m = 0$ curves shown in Figure 1. Clearly, to obtain a more precise description of the cross section, data at higher temperatures are needed. To accomplish this the data sets of Masten, Bowman, and Hanson and Du and Hessler were added to the previous set. These data, their best-fit curve, and the 95.4% confidence envelope are shown in Figure 5. The best-fit parameters from this full set of data give

$$\ln\{k_{fwd}(\mathrm{cm^3\,s^{-1}})\} = -(18.95 \pm 0.24) - (0.406 \pm 0.030)\ln\{T(\mathrm{K})\} - (8354 \pm 30)/T(\mathrm{K}) \quad (26)$$

Again, the uncertainties are the standard deviation calculated from the Monte Carlo simulations. A careful comparison of Figures 4 and 5 shows that the vast majority of the higher temperature data fall within the confidence envelope of the

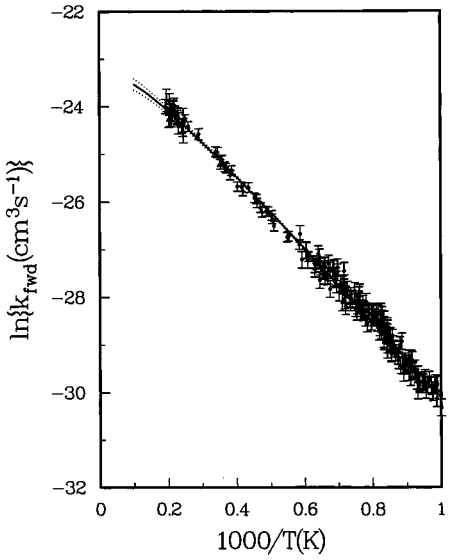

Figure 5. Full data set for the rate of the reaction H + O_2 → OH + O. The solid line represents eq 26 and the dotted lines the 95.4% confidence envelope. The data are from refs 41−43 and Table 1. See the text for details.

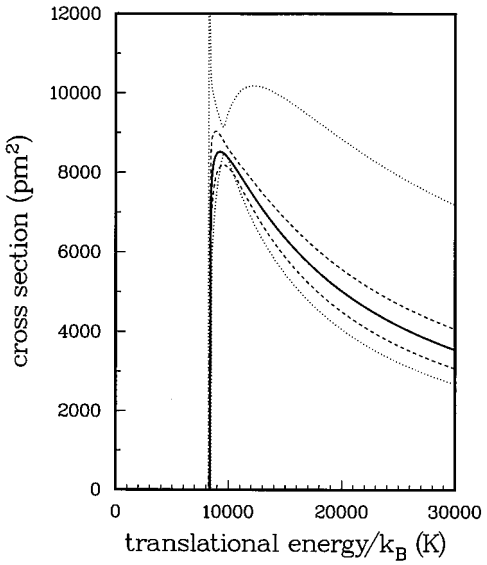

Figure 6. Comparison of confidence envelopes calculated from the two different sets of data shown in Figures 4 and 5. The dotted lines represent the 68.3% confidence envelope calculated from the lower temperature data only, Figure 4, and the dashed lines represent the 68.3% confidence envelope calculated from the full data set, Figure 5. The solid line is calculated from the parameters of eq 26.

lower-temperature data, that both the best-fit curve and confidence envelope of Figure 5 fall within the confidence envelope of Figure 4, and, most importantly, that the confidence envelope of Figure 5 is significantly smaller than the one in Figure 4. Furthermore, a comparison of the parameters in eqs 25 and 26 demonstrates that the addition of high-temperature data refines the parameters, *i.e.*, the parameters of eq 26 fall within the standard deviations of the parameters of eq 25 and the standard deviations in eq 26 are smaller than in eq 25. Inspection of Table 3 shows that in both cases the values of χ^2_{red} are less than 1.0. Therefore, we can say all of the 223 points between 158 and 5170 K can be described by a single rate expression that contains only three parameters. Equally significant are the facts that the histogram of the normalized residuals is Gaussian with a standard deviation of 0.97 and that systematic deviations cannot be identified. Therefore, any assertion that the rate coefficient must be described by a sum of rate coefficients is not supported by experimental data. This does not imply that the rate coefficient cannot be described by a sum of partial rate coefficients. However, it does imply that there is a relatively tight confidence envelope that any sum of partial rate coefficients must fall within. Later, we will discuss the implications of this for the cross section.

The influence of additional information about the rate coefficient on calculations of the thermally-averaged cross section is shown in Figure 6. Here the 68.3% confidence envelopes for both of the above calculations are shown. The dotted lines represent the confidence envelope from the lower temperature data, Figure 4, and the dashed lines the confidence envelope for the full set of data, Figure 5. The solid line represents the thermally averaged cross sections calculated with the parameters of eq 26. The upper dotted line indicates the possible singular behavior of the lower temperature data set. Recall, in general it is not possible to write a simple analytic expression for the confidence envelope. Perhaps the most significant aspect of Figure 6 is not that the confidence envelope is reduced when higher-temperature data are added, but that the confidence envelopes provide a realistic description of the range of possible values of the cross section. Clearly, if the lower temperature data were the only available data our experimental knowledge of the cross section would be limited.

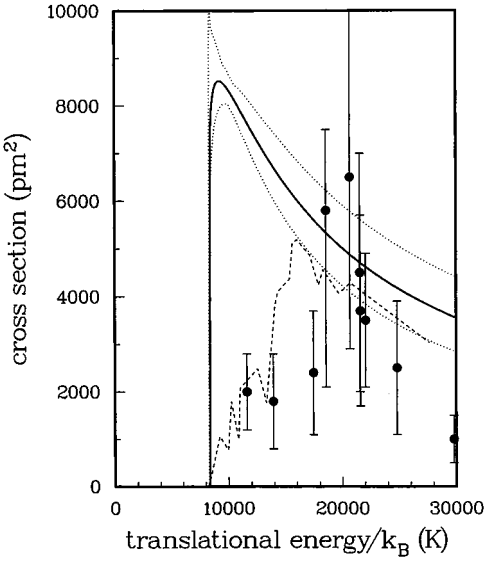

Figure 7. Comparison of the cross section for the reaction H + O_2 → OH + O. The solid line is calculated from the parameters of eq 26 and the dotted lines represent the 95.4% confidence envelope. The points are the measurements from refs 45 and 46 and the dashed line represents the theoretical calculation of ref 47.

As was shown previously, the cross section calculated from the experimental data may be compared to calculated cross sections and, if available, measured cross sections. To illustrate this, the thermally averaged cross section calculated from the parameters of eq 26 and its 95.4% confidence envelope are given in Figure 7. The points in this figure are the measurements performed by Wolfrum's group[45,46] and the dashed line is the theoretical calculation of Varandas.[47] It is tempting to compare the measured cross sections to the thermally averaged cross section determined from the kinetic data. However, this comparison would not be valid. Although the translational energies of the hydrogen atoms used to measure the cross sections were very high, the vibrational temperature of the oxygen molecules was near room temperature, $T_{int} \sim 294$ K. Similarly, the classical trajectory calculations performed by

Varandas were also limited to the ground vibrational level.[47] Zhang and Zhang have performed time-dependent quantum wave packet calculations for $v = 0$, 1, 2, and 3 on the same surface.[48] They find that rovibrational excitation gradually decreases the probability amplitude. However, they also point out that, when measured in kinetic energies, this does not imply that excitation decreases reaction probability. For completeness we note that Leforestier and Miller calculated the cumulative reaction probability for this reaction,[49] Yang and Klippenstein have compared statistics and dynamics,[50] Pack, Butcher, and Parker have computed three-dimensional quantum probabilities,[51] and Miller and Garrett have quantified the non-RRKM behavior.[52] Any detailed discussion of these or other works goes beyond the scope of this article.

Before concluding this illustration we must discuss the implications for the cross sections that are often calculated for specific internal states such as vibrational or rotational states. Simply stated, it is very difficult, although not impossible, to extract information about specific internal states from thermal kinetic data. If the cross sections and, therefore, the rate coefficients associated with different internal states are significantly different, then precise kinetic data over a sufficiently large temperature range will force the experimentalist to describe the date in terms of two or more parallel channels. To the extent that the data demand a multichannel description, the parameters associated with these channels may be determined along with the uncertainties. In the above illustrations the data did not indicate that a multichannel description is needed. Therefore, we cannot make any statements about the rate coefficients or cross sections associated with individual internal states. However, we can make statements about the thermally averaged rate coefficients and cross sections. In particular, eqs 3 and 4 give the thermally averaged rate coefficients and cross sections in terms of rate coefficients and cross sections associated with specific internal states. The uniqueness theorem of Laplace transforms[53] and their linear property require that each cross section associated with an internal state has a rate coefficient that is associated with the same internal state. Furthermore, the thermally averaged rate coefficient and cross section derived from the rate coefficients and cross sections of the internal states must fall within the confidence envelopes calculated from the kinetic data. Therefore, since the measured and calculated cross sections shown in Figure 7 are associated only with the ground vibrational level of molecular oxygen, we can conclude that higher vibrational levels of molecular oxygen must make a significant contribute to the thermally averaged cross section just above the threshold of 8354 K. Furthermore, above $\epsilon_t/k_B = 18\,000$ K Wolfrum's measured cross sections and Varanda's calculated cross section tend to fall within the 95.4% confidence envelope of the thermally averaged cross section. Therefore, we may anticipate that the cross sections from higher vibrational levels of molecular oxygen will not contribute significantly above $\epsilon_t/k_B = 18\,000$ K. At the present time, we have extracted all of the information that may be extracted from the thermal kinetic data.

B. Associative Reaction. To illustrate the properties of associative reactions, consider methyl−methyl association to form ethane. Previously,[14] we demonstrated that the high-pressure rate coefficient follows Berthelot's equation and is given by

$$k^{\infty}_{asso}(\mathrm{cm^3\ s^{-1}}) = 8.78 \times 10^{-11} \exp[(-1.38 \times 10^{-3})T(\mathrm{K})] \quad (27)$$

The high-pressure rate data, best-fit curve, and 95.4% confidence envelope are shown in Figure 8. The microcanonical rate for an internal temperature of 500 K and its 95.4% confidence envelope are shown in Figure 9. The microcanonical rates calculated from eq 19 for 200, 1000, and 2000 K are shown in Figure 10. For each of these, the effective barrier heights, E_{eff}/hc, are 38.4, 959, and 3836 cm^{-1}, respectively. When eq 13 is used to calculate the macroscopic rates, the microcanonical rates shown in Figure 10 reproduce the experimental data.

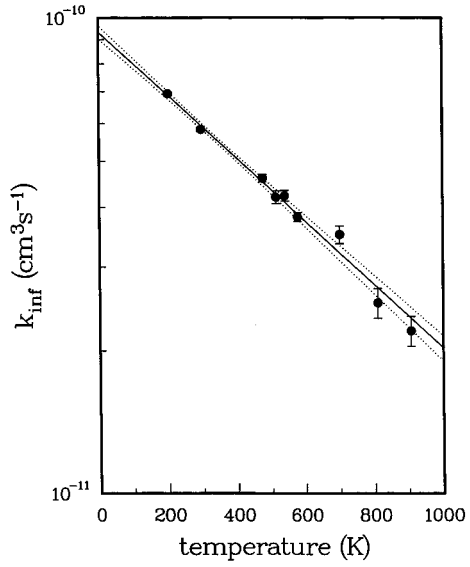

Figure 8. High-pressure associative rate coefficients for $CH_3 + CH_3 \rightarrow C_2H_6$ from ref 30. The solid line represents the parameters of eq 27 and the dotted lines the 95.4% confidence envelope.

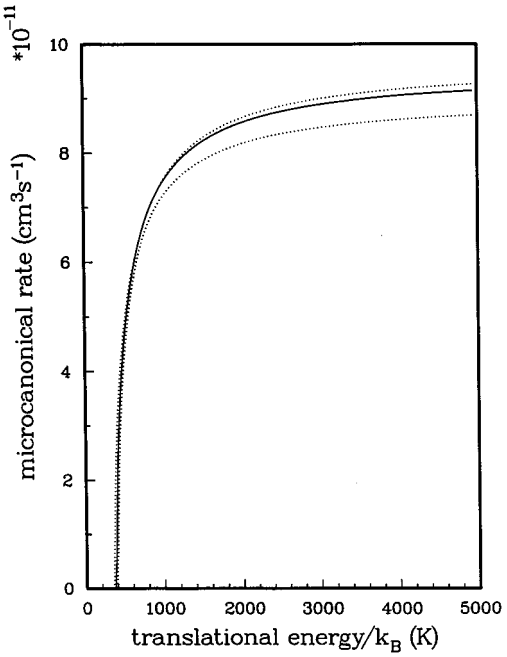

Figure 9. Microcanonical rate and confidence envelope calculated from Figure 8. The internal temperature of the methyl radicals is 500 K. This gives an effective threshold of $E_{eff}/k_B = 345$ K.

It is instructive to compare the microcanonical rate presented above with rates calculated from a potential energy surface. Fortunately, Harding has recently performed ab initio calculations of the potential energy surface at the CAS+1+2/cc-pdz level.[18] Approximately 8000 randomly chosen points have been calculated. Klippenstein used these ab initio points in a direct variational RRKM calculation of the E and J resolved rate, $k(E, J)$, of the dissociation of ethane.[17] Here, E is the total

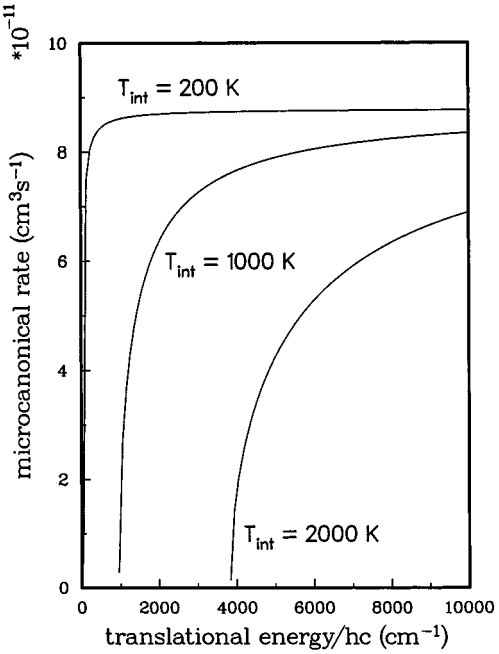

Figure 10. Microcanonical rates as a function of translational energy, ϵ_t/hc, for the association of two methyl radicals to form ethane. Three different internal temperatures are shown. See the text for parameters and details.

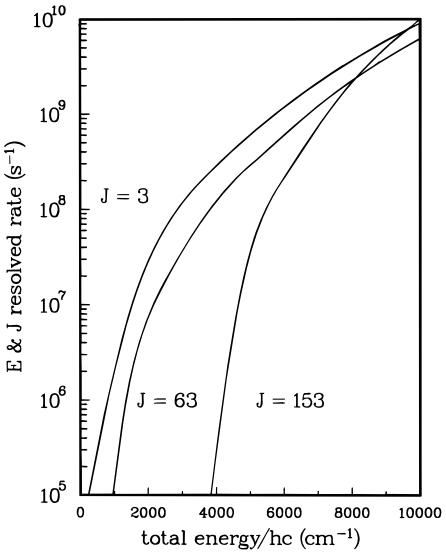

Figure 11. Calculated resolved rates, $k(E, J)$, for the dissociation of ethane.[17,18] The energy is the vibrational plus rotational plus translational energy of the methyl radicals and J is the total angular momentum of the system. J values of 63 and 153 correspond to the effective thresholds at 1000 and 2000 K shown in Figure 10.

energy of the system, vibrational plus rotational plus translational, and J is its total angular momentum. Preliminary results for $J = 3$, 63, and 153 are shown in Figure 11. Of course, microscopic reversibility must be used to convert the curves in Figure 11 into analogous curves for the associative reaction. However, we note that the threshold for dissociation increases as the angular momentum increases. Therefore, the description that emerges from these preliminary calculations is that as the internal energy of the associating/dissociating species increases the effective angular momentum of the system also increases and, thereby, the effective threshold to association/dissociation increases. Furthermore, the effective threshold of 959 cm^{-1} at 1000 K corresponds to a J of 63 and the effective threshold of 3836 cm^{-1} at 2000 K corresponds to a J of 153. The facts that (1) the microcanonical rate calculated from kinetic data has an effective threshold that depends upon the internal temperature and (2) *k(E, J)* resolved rates calculated from a state-of-the-art potential energy surface and sophisticated dynamical calculations also have an effective threshold that depends upon J support the assumption that eq 9 is valid and encourage additional investigations.

IV. Discussion

The phenomenological equations derived here are based on the assumptions that van't Hoff's four-parameter equation reproduces the kinetic data and that the height of the effective threshold in his equation can be expressed as a function of the internal temperature of the reactants. Then the phenomenological equations for the reactive cross section and microcanonical rate follow directly from the mathematical properties of the Laplace transform. Sometimes, the assertion is made that van't Hoff's equation is not unique and that the temperature-dependent rate coefficient could be described by any number of other equations. This may be true! However, any alternate description must provide an equal or superior reproduction of the data. The uniqueness theorem of the Laplace transform[53] implies that the cross section calculated by an alternate description will fall within the confidence envelope calculated from van't Hoff's equation. Therefore, the fact that an alternate description may exist is irrelevant. For an alternate description to be useful it must provide a better representation of the data or a comparable representation with an alternate physical description. For example, in a subsequent paper we derive two new empirical rate expressions for reactions that proceed on barrierless potential energy surfaces.[38] These equations accommodate the quantum threshold behavior that controls the reaction as the temperature approaches zero. Previously, only Berthelot's equation, which is contained within van't Hoff's equation, could accommodate the low-temperature quantum threshold behavior.

By transforming the information contained in the kinetic data into reactive cross sections for the forward and reverse reactions of $H + O_2 \leftrightarrow OH + O$ and comparing them to calculated cross sections it is apparent that additional theoretical work is warranted. Similarly, from the study of the $CH_3 + CH_3$ system the important role of angular momentum in the dissociative and associative reactions has been identified. Another question one may ask is, what is the relationship of the effective threshold to the transition state in flexible transition state calculations? One may conclude from these examples that the transformed descriptions of the kinetic data, in terms of an energy-dependent reactive cross section or microcanonical rate, provide a useful tool for both experimental and theoretical kineticists. It is hoped that this work will motivate additional questions, detailed calculations, and additional comparisons with experimental data.

Acknowledgment. This article represents an attempt to answer a question posed by Michael J. Pilling and Struan J. Robertson at the 14*th* International Symposium on Gas Kinetics. They are thanked for the stimulating discussions that occurred at this symposium. Lawrence B. Harding and Stephen J. Klippenstein are thanked for sharing their unpublished calculations. I also thank Stephen K. Gray, Stephen J. Klippenstein, George C. Schatz, and Albert F. Wagner for helpful discussions and an anonymous reviewer for asking about the reverse reaction. This work was performed under the auspices of the U.S. Department of Energy, Office of Energy Research, Division of Chemical Sciences.

References and Notes

(1) Pilling, M. J.; Smith, I. W. M. *Modern Gas Kinetics: theory, experiment, and application*; Blackwell Scientific Publications: Oxford, United Kingdom, 1987; pp 190−205.
(2) Shepard, R.; Shavitt, I.; Pitzer, R. M.; Comeau, D. C.; Pepper, M.; Lischka, H.; Szalay, P. G.; Ahlrichs, R.; Brown, F. B.; Zhao, J. *Int. J. Quantum Chem., Quantum Chem. Symp.* **1988**, *S22*, 149−165.
(3) Truhlar, D. G.; Isaacson, A. D.; Garrett, B. C. In *Theory of Chemical Reaction Dynamics*; Baer, M., Ed.; CRC: Boca Raton, FL, 1985; Vol. 4, pp 65.
(4) Wardlaw, D. M.; Marcus, R. A. *Adv. Chem. Phys.* **1988**, *70* (I), 231−263.
(5) Miller, W. H.; Schwartz, S. D.; Tromp, J. W. *J. Chem. Phys.* **1983**, *79*, 4889−4898.
(6) Klippenstein, S. J. *J. Chem. Phys.* **1992**, *96*, 367−371.
(7) Yamamoto, T. *J. Chem. Phys.* **1960**, *33*, 281−291.
(8) Miller, W. H. *J. Chem. Phys.* **1974**, *61*, 1823−1834.
(9) Newman, D. J. *Aust. J. Phys.* **1978**, *31*, 489−513.
(10) Menzinger, M.; Wolfgang, R. *Angew. Chem. internat. Edit.* **1969**, *8*, 438−444.
(11) LeRoy, R. L. *J. Phys. Chem.* **1969**, *73*, 4338−4344.
(12) Laidler, K. J. *The World of Physical Chemistry*; Oxford University Press: Oxford, England, 1993; pp 233−289.
(13) Polanyi, J. C.; Schreiber, J. L. In *Physical Chemistry, An Advanced Treatise*; Jost, W., Ed.; Academic Press, Inc.: New Nork, 1974; number VIA, Kinetics of Gas Reactions, pp 383−487.
(14) Hessler, J. P. *Int. J. Chem. Kinet.* **1997**, *29*, 803−817.
(15) Laidler, K. J. *Chemical Kinetics*, 3rd ed.; Harper and Row, Pub. Inc.: New York, 1987; pp 40−46.
(16) Hessler, J. P.; Ogren, P. J.; Current, D. H. *Comput. Phys.* **1996**, *10*, 186−199.
(17) Klippenstein, S. J., April, 1997. Personal communication.
(18) Harding, L. B., April, 1997. Personal communication.
(19) Mott, N. F.; Massey, H. S. W. *The Theory of Atomic Collisions*, 2nd ed.; The Clarendon Press: Oxford, England, 1949.
(20) Blatt, J. M.; Weisskopf, V. F. *Theoretical Nuclear Physics*; John Wiley and Sons, Inc.: New York, 1952.
(21) Eliason, M.; Hirschfelder, J. O. *J. Chem. Phys.* **1959**, *30*, 1426−1436.
(22) Laidler, K. J. *Chemical Kinetics*, 3rd ed.; Harper and Row, Publishers, Inc.: 1987; pp 84−87.
(23) Levine, R. D.; Bernstein, R. B. *Molecular Reaction Dynamics and Chemical Reactivity*; Oxford University Press: Oxford, England, 1987; p 36.
(24) Abramowitz, M.; Stegun, I. A. *Handbook of Mathematical Functions With Formulas, Graphs, and Mathematical Tables*; U. S. Department of Commerce, National Bureau of Standards: Washington, DC, 1964; pp 1020−1030.
(25) Wigner, E. P. *Phys. Rev.* **1948**, *73*, 1002−1009.
(26) Craig, I. J. D.; Thompson, A. M. *Comput. Phys.* **1995**, *8*, 648−654.
(27) Pilling, M. J.; Seakins, P. W. *Reaction Kinetics*; Oxford University Press: Oxford, England, 1995; pp 138−141.
(28) Miller, W. H. *J. Chem. Phys.* **1995**, *99*, 12 387−12 390.
(29) Pawlowska, Z.; Gardiner, W. C.; Oref, I. *J. Phys. Chem.* **1993**, *97*, 5024−5031.
(30) Hessler, J. P. *J. Phys. Chem.* **1996**, *100*, 2141−2144.
(31) Robertson, S. H.; Pilling, M. J.; Baulch, D. L.; Green, N. J. B. *J. Phys. Chem.* **1995**, *99*, 13452−13460.
(32) Lewis, R. S.; Watson, R. T. *J. Phys. Chem.* **1980**, *84*, 3495−3503.
(33) Howard, M. J.; Smith, I. W. M. *J. Chem. Soc. Faraday Trans. 2* **1981**, *77*, 997−1008.
(34) Brune, W. H.; Schwab, J. J.; Anderson, J. G. *J. Phys. Chem.* **1983**, *87*, 4503−4514.
(35) Smith, I. W. M.; Stewart, D. W. A. *J. Chem. Soc. Faraday Trans.* **1994**, *90*, 3221−3226.
(36) Clary, D. C.; Werner, H. J. *Chem. Phys. Lett.* **1984**, *112*, 346−350.
(37) Graff, M. M.; Wagner, A. F. *J. Chem. Phys.* **1990**, *92*, 2423−2439.
(38) Hessler, J. P. *J. Phys. Chem*., submitted for publication.
(39) Marques, J. M. C.; Wang, W.; Varandas, A. J. C. *J. Chem. Soc. Faraday Trans.* **1994**, *90*, 2189−2200.
(40) Chase, M. W., Jr.; Davies, C. A.; Downey, J. R., Jr.; Frurip, D. J.; McDonald, R. A.; Syverd, A. N. *J. Phys. Chem. Ref. Data* **1985**, *14*, Suppl. 1.
(41) Pirraglia, A. N.; Michael, J. V.; Sutherland, J. W.; Klemm, R. B. *J. Phys. Chem.* **1989**, *93*, 282−291.
(42) Masten, D. A.; Hanson, R. K.; Bowman, C. T. *J. Phys. Chem.* **1990**, *94*, 7119−7128.
(43) Du, H.; Hessler, J. P. *J. Chem. Phys.* **1992**, *96*, 1077−1092.
(44) Ryu, S. O.; Hwang, S. M.; Rabinowitz, M. J. *J. Phys. Chem*. **1995**, *99*, 13 984−13 991.
(45) Kessler, K.; Kleinermanns, K. *J. Chem. Phys.* **1992**, *97*, 374−377.
(46) Seeger, S.; Sick, V.; Volpp, H.; Wolfrum, J. *Isr. J. Chem.* **1994**, *34*, 5−18.
(47) Varandas, A. J. C. *Mol. Phys.* **1995**, *186*, 1159−1164.
(48) Zhang, D. H.; Zang, J. H. *J. Chem. Phys.* **1994**, *101*, 3671−3678.
(49) Leforestier, C.; Miller, W. H. *J. Chem. Phys.* **1994**, *100*, 733−735.
(50) Yang, C.; Klippenstein, S. J. *J. Chem. Phys.* **1995**, *103*, 7287−7298.
(51) Pack, R. T.; Butcher, E. A.; Parker, G. A. *J. Chem. Phys.* **1995**, *102*, 5998−6012.
(52) Miller, J. A.; Garrett, B. C. *Int. J. Chem. Kinet.* **1997**, *29*, 275−287.
(53) Kuhfittig, P. K. F. *Introduction to the Laplace Transform*; Plenum Press: New York, 1978.